PRKDC Induces Chemoresistance in Osteosarcoma by Recruiting GDE2 to Stabilize GNAS and Activate AKT

Wenchao Zhang[1,2], Wei Li[3], Chi Yin[1,2], Chengyao Feng[1,2], Binfeng Liu[1,2], Haodong Xu[1,2], Xin Jin[3], Chao Tu[1,2,5], and Zhihong Li[1,2,4,6]

ABSTRACT

Chemoresistance is one of the major causes of poor prognosis in osteosarcoma. Alternative therapeutic strategies for osteosarcoma are limited, indicating that increasing sensitivity to currently used chemotherapies could be an effective approach to improve patient outcomes. Using a kinome-wide CRISPR screen, we identified PRKDC as a critical determinant of doxorubicin (DOX) sensitivity in osteosarcoma. The analysis of clinical samples demonstrated that PRKDC was hyperactivated in osteosarcoma, and functional experiments showed that the loss of PRKDC significantly increased sensitivity of osteosarcoma to DOX. Mechanistically, PRKDC recruited and bound GDE2 to enhance the stability of protein GNAS. The elevated GNAS protein levels subsequently activated AKT phosphorylation and conferred resistance to DOX. The PRKDC inhibitor AZD7648 and DOX synergized and strongly suppressed the growth of osteosarcoma in mouse xenograft models and human organoids. In conclusion, the PRKDC-GDE2-GNAS-AKT regulatory axis suppresses DOX sensitivity and comprises targetable candidates for improving the efficacy of chemotherapy in osteosarcoma.

Significance: Targeting PRKDC suppresses AKT activation and increases sensitivity to doxorubicin in osteosarcoma, which provides a therapeutic strategy for overcoming chemoresistance.

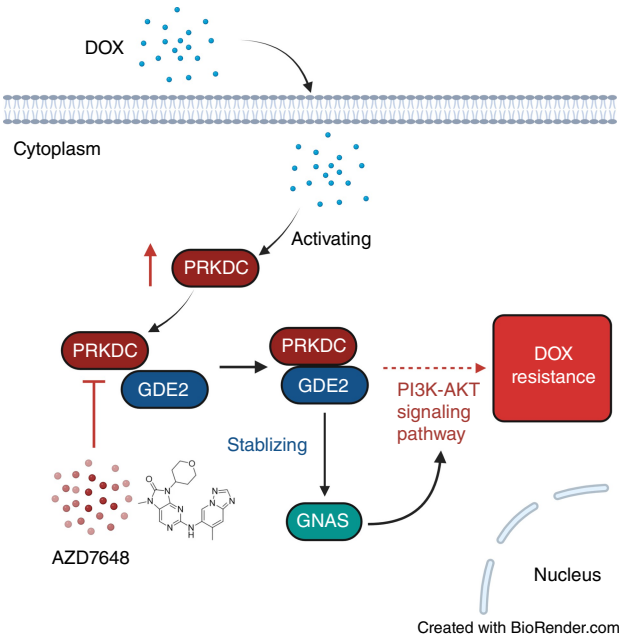

Introduction

Osteosarcoma is the most common form of primary bone malignancy worldwide, mostly occurring in adolescents and children (1, 2). The mainstay of osteosarcoma treatment is surgery and combined neoadjuvant chemotherapy, in which the backbone of first-line chemotherapy comprises doxorubicin (DOX), cisplatin, methotrexate, and ifosfamide. Despite increased understanding of the tumor microenvironment (3–5) and molecular pattern (6–8), the prognosis for osteosarcoma has not improved over the last 2 decades (9). The development of drug resistance is the most common driver of unfavorable outcomes (10). In patients with drug-resistant disease, additional doses or drugs could not markedly improve prognosis because of the occurrence of local recurrence and metastasis (11). Therefore, an urgent clinical need to reveal the underlying mechanisms of drug resistance and exploit new strategies to increase drug sensitivity is observed.

DOX, a member of the anthracycline family, suppresses tumor growth by interacting with DNA and DNA topoisomerase II (12). The chemoresistance of DOX involves various molecular mechanisms, including drug efflux (13), enhancement of DNA repair (14), metabolic alteration (15), and activation of kinase-related pathways. It is well documented that the PI3K/AKT pathway mediates resistance to DOX (16, 17). DOX induced AKT activation and

[1]Department of Orthopedics, The Second Xiangya Hospital, Central South University, Changsha, China. [2]Hunan Key Laboratory of Tumor Models and Individualized Medicine, The Second Xiangya Hospital, Changsha, China. [3]Department of Urology, The Second Xiangya Hospital, Central South University, Changsha, China. [4]Shenzhen Research Institute of Central South University, Guangdong, China. [5]Changsha Medical University, Changsha, China. [6]FuRong Laboratory, Changsha, China.

W. Zhang and W. Li contributed equally to this article.

Corresponding Authors: Xin Jin, Department of Urology, The Second Xiangya Hospital, Central South University, 139 RenMin Road, Changsha 410011, China. E-mail: jinxinxy2@csu.edu.cn; and Chao Tu, Department of Orthopedics, The Second Xiangya Hospital, Central South University, 139 RenMin Road, Changsha 410011, China. E-mail: tuchao@csu.edu.cn; and Zhihong Li, E-mail: lizhihong@csu.edu.cn

Cancer Res 2024;84:2873–87

doi: 10.1158/0008-5472.CAN-24-0163

PI3K/AKT inhibitors, which dramatically enhances its cytotoxicity. Several molecules have been demonstrated to regulate the PI3K/AKT pathway to mediate DOX sensitivity. UDP-glucose ceramide glucosyltransferase, a key enzyme for the synthesis of glycosylated sphingolipids, activates AKT by altering the composition of glycosphingolipid-enriched microdomains (18). LRP1B directly binds to NCSTN and regulates its protein expression, subsequently modulating the PI3K/AKT pathway and affecting the DOX resistance (19). Thus, further exploration of the regulatory network of the PI3K/AKT pathway could provide novel targets for the reversion of DOX resistance in osteosarcoma.

PRKDC encodes the catalytic subunit of DNA-dependent protein kinase (DNA-PK), which is a serine/threonine–protein kinase that plays a critical role in cancer biology. Evidence has shown that PRKDC is overexpressed and phosphorylated in various solid tumors, leading it to be proposed as a potential therapeutic target (20, 21). More recently, PRKDC has been identified as a critical modulator of tumor sensitivity to radiotherapy and DNA-damaging agents (22–24). PRKDC also participates in the innate immune response, and targeting PRKDC could improve checkpoint blockade immunotherapy (25). Despite the crucial role of PRKDC in the cellular processes and drug resistance of cancers, the underlying mechanism remains unclear.

Glycerophosphodiester phosphodiesterase 2 (GDE2), also known as glycerophosphodiester phosphodiesterase domain containing 5, is a six-transmembrane protein that engages in neuronal differentiation (26). Matas-Rico and colleagues found that GDE2 promoted neuroblastoma differentiation and was associated with poor prognosis (27). Since then, GDE2 has been illustrated as a critical driver for various tumors, including colorectal cancer (28), nasopharyngeal carcinoma (29), and gastric cancer (30). Furthermore, GDE2 was reported to mediate 5-Fu and cisplatin resistance (28, 29), but the regulatory mechanism remains unclear and needs further exploration. Guanine nucleotide-binding protein-G(S) subunit alpha (GNAS) encoding the alpha-subunit of the stimulatory G protein (Gsα) was originally discovered to regulate neurotransmitters and many hormones (31). Recently, GNAS mutants were reported to drive tumorigenesis of pancreatic cancer by modulating PKA-mediated SIK suppression (32). Moreover, the activating mutants of GNAS have been demonstrated to be linked to a subgroup of inflammatory liver tumors with STAT3 activation (33). GNAS has also been shown to be genetically activated in a small subset of small cell lung cancer, in which it promotes tumor progression via the PKA/PP2A axis (34). However, whether GNAS is associated with chemoresistance in cancer remains unclear.

In this study, we identified PRKDC as a critical driver of doxorubicin (DOX) sensitivity in osteosarcoma through a CRISPR screen. In terms of the underlying mechanism, our results revealed that PRKDC was highly activated in DOX-treated cells and chemoresistant osteosarcoma. We demonstrated that PRKDC could activate the PI3K/AKT pathway by recruiting GDE2 to stabilize GNAS, which ultimately resulted in DOX resistance in osteosarcoma. These findings, for the first time, suggest that the PRKDC/GDE2/GNAS/AKT axis has a critical role in regulating DOX sensitivity in osteosarcoma and provides novel targets for enhancing DOX sensitivity.

Materials and Methods

Clinical specimens

Osteosarcoma samples were collected from The Second Xiangya Hospital, Central South University. Written informed consent was acquired from all patients before surgery. The studies were conducted in accordance with recognized ethical guidelines (Declaration of Helsinki) and approved by the Ethics Committees of The Second Xiangya Hospital (Approval No. 2023-Z0477).

We collected specimens of needle biopsy and surgical resection from patients diagnosed with osteosarcoma before and after standard MAP chemotherapy (consisting of methotrexate, DOX, and cisplatin). The treatment efficacy was assessed by CT or MRI according to RECIST 1.1 (35). Specimens from patients with progressive disease and partial response were collected for further analysis. We defined patients who achieved a partial response as chemotherapy sensitivity and patients with progressive disease as chemoresistance.

Cell lines and cell culture

The 143B, HOS, U2OS, MG63, A549, PC-9, HepG2, Hep3B, 22Rv1, C4-2, and HEK293T cell lines were purchased from Procell Life Science & Technology Co., Ltd. The 143B and HEK293T cells were cultured in DMEM medium (Procell Life Science & Technology); the HOS, MG63, HepG2, and Hep3B cells were cultured in MEM (Procell Life Science & Technology); the A549, PC-9, 22Rv1, and C4-2 cells were cultured in RPMI1640 medium (Procell Life Science & Technology); and the U2OS cells were cultured in McCoy's 5A medium. All culture medium was supplemented with 10% fetal bovine serum (FBS; NEWZERUM Ltd.). All cells were incubated at 37°C in 5% CO_2. Cells were tested for *Mycoplasma* contamination every 3 months using the TransDetect PCR Mycoplasma Detection Kit (TransGen Biotech). All cell lines were identified using short tandem repeat profiling.

Quantitative real-time PCR

Total RNA was extracted from osteosarcoma cells using a standard TRIzol (Thermo Fisher Scientific) protocol. Nano-Drop 2000 (Thermo Fisher Scientific) was used to measure the concentration and quality of RNA. RNA was reverse-transcribed and amplified using Hifair III Reverse Transcriptase (Yeasen Biotechnology Co., Ltd.). RT-qPCR reactions were performed on Quantstudio5 (Applied Biosystems) using SYBR Green Master Mix (#AG11746, Accurate Biology). The relative gene expression levels were calculated by the $2^{-\Delta C_t}$ method after normalizing to GAPDH levels. The sequences of all primers are provided in Supplementary Table S1.

Western blotting

Cells were lysed with RIPA buffer (#P0013, Beyotime), and the protein concentration was measured using a Micro BCA Protein Assay Kit (Sigma-Aldrich). Subsequently, the proteins were separated by SDS-PAGE and electroblotted onto PVDF membranes. The membrane was blocked with 5% skimmed milk and incubated with the corresponding primary antibody at 4°C overnight. After washing with TBST three times, the membrane was incubated with a secondary antibody for 1 hour at room temperature. The membrane was then washed three times with TBST, and enhanced chemiluminescence (ECL) was added dropwise onto the PVDF membrane. The protein signal was detected by Bio-Rad Image Lab.

The following antibodies were used: DNA-PKcs (#ab32566, abcam, 1:5,000 dilution); DNA-PKcs S2056 (#ab124918, abcam, 1:5,000 dilution); pAKT-S473 (#4060S, Cell Signaling Technology, 1:1,000 dilution); pAKT-T308 (#13038, Cell Signaling Technology, 1:1,000 dilution); ENO1 (#11204–1-AP, Proteintech, 1:2,000 dilution); GDE2 (#25703-1-AP, Proteintech, 1:2,000 dilution); GNAS (#10150–2-AP, Proteintech, 1:1,000 dilution); beta-actin (#66009–1-Ig, Proteintech,

1:5,000 dilution); GAPDH (#60004-1-Ig, Proteintech, 1:5,000 dilution); BAX (#50599-2-Ig, Proteintech, 1:1,000 dilution); BCL2 (#68103-1-Ig, Proteintech, 1:1,000 dilution); HRP conjugated goat-anti-mouse antibody (#511103, Zenbio, 1:10,000 dilution); and HRP conjugated goat-anti-rabbit antibody (#511203, Zenbio, 1:10,000 dilution).

Colony formation assay

For the colony formation assay, osteosarcoma cells were seeded into six-well plates at a concentration of 1000 cells per well. The cells were then cultured for 2 weeks until a colony was clearly formed. The cells were washed with PBS three times and stained with 0.1% crystal violet. The number of colonies was counted using ImageJ software.

CCK-8 assay

The CCK-8 assay was conducted as previously reported (36). In brief, osteosarcoma cells were seeded into 96-well plates at a concentration of 2000 cells per well and incubated overnight. Corresponding drugs were added into each well and incubated for the indicated time. Next, 10 μL of sterile CCK-8 was added to each well and incubated at 37°C for 1 hour before measuring the absorbance at 450 nm.

Transfection of siRNA and plasmids

The siRNAs or plasmids were incubated with Lipofectamine 2000 (Thermo Fisher Scientific) in serum-free Opti-MEM medium for 15 min. Then, the mixture was carefully added to plates or dishes. After 6 hours of transfection, the Opti-MEM medium was replaced with complete DMEM. Cells were collected 72 hours after transfection for follow-up experiments. The siRNA sequences of PRKSC, GDE2, and GNAS are listed in Supplementary Table S1.

Lentivirus construction and transduction

To establish a stable CRISPR/Cas9 knockout cell line, sgRNA plasmids were co-transfected with package plasmids (pMD2.G and psPAX2) into HEK293T cells using lipo2000 (Thermo Fisher Scientific). After 48 hours, the supernatant was collected and concentrated using Amicon Ultra Centrifugal Filters (Millipore). For viral transduction, the virus was added to the culture medium with Polybrene (Beijing Solarbio Science & Technology). After 48 hours of transduction, the cells were selected with 2 μg/mL puromycin for 7 days. LentiCRISPR v2 (#52961, Addgene) was provided by Feng Zhang's laboratory. The PRKDC sgRNA sequences were obtained from our customized Human Brunello kinome pooled library (SYNBIO Technologies) and are provided in Supplementary Table S2.

Kinome-wide CRISPR/Cas9 knockout library screen

The human kinome CRISPR knockout library was customized by SYNBIO Technologies. This library targets 507 human kinases. For each gene, 10 corresponding sgRNAs were designed and synthesized. A total of 164 sgRNAs that did not target any gene were used as controls. The sequences of all sgRNAs are provided in Supplementary Table S2. The workflow of the CRISPR screen is illustrated in **Fig. 1A**. In brief, cells were transduced with the kinome CRISPR knockout library at a low MOI of 0.3 and coverage of 500×. The transduced cells were then selected with 2 μg/mL puromycin for 7 days to remove the negative cells. The mutant cell pool was treated with DOX (0.1 μmol/L) or DMSO for another 7 days. At the end of treatment, 3×10^6 cells were collected from each group for DNA extraction. The sgRNAs were amplified using NEBNext High-Fidelity 2× PCR Master Mix and sequenced by Genergy Biotechnology. The results were analyzed using the MAGeCK v0.5.7 algorithm (37).

Immunohistochemistry

Paraffin-embedded sections of clinical and mouse samples were used for IHC staining following a previously reported protocol. The clinical samples were stained with DNA-PKcs S2056 (#ab124918, Abcam), and the mouse samples were stained with Ki-67 (#ab16667, Abcam) and cleaved caspase-3 (#9661, Cell Signaling Technology). The IHC scores were independently assessed by two senior pathologists using a previously reported scoring method (38).

Flow cytometry

The Annexin V-FITC/propidium iodide (PI) assay was used to measure the apoptosis rate according to the manufacturer's instructions. Briefly, cells were stained with Annexin V-FITC and PI from the Annexin V-PE/PI Apoptosis Detection Kit (#40302ES60, YEASEN) for 10 minutes before detecting using a Cytek NL-CLC. For Ki-67 detection, cells were fixed and permeated using the eBioscience Foxp3/Transcription Factor Staining Buffer Set (Invitrogen) before staining with Ki-67 antibodies (Biolegend) for 30 min. To detect cell surface markers, cells were directly incubated with APC anti-CD11b (#101211, Biolegend), APC/Fire anti-CD45 (103153, Biolegend), and PE anti-CD3 antibodies (#100205, Biolegend) for 30 min at 4°C. After washing three times, the cells were subjected to flow cytometry analysis. FlowJo software (FlowJo) was used to analyze the data.

Comet assay

The comet assay was conducted as previously reported (39). In brief, cells were digested and mixed with low-melting point agarose before spreading the cell suspension onto a microscope slide pre-coated with a thin layer of agarose. The cells were then lysed and subjected to electrophoresis in an alkaline buffer. After neutralization, DNA was stained using PI (#C2041S-5, Beyotime), and the DNA fragments were visualized under a fluorescence microscope.

Coimmunoprecipitation and liquid chromatography coupled to tandem mass spectrometry

Total proteins were extracted using IP buffer and incubated with protein A + G beads (#P2029, Beyotime) and IgG (#A7007, Beyotime) or primary antibody for 24 hours. The beads were collected and washed with PBS three times. After boiling with an SDS-loading buffer for 10 minutes, the eluted protein was analyzed by gel electrophoresis and liquid chromatography–tandem mass spectrometry (LC–MS/MS).

Mouse xenograft assay

All animal experiments were approved by the Institutional Animal Care and Use Committee of The Second Xiangya Hospital, Central South University under Approval No. 20230301. BALB/c nude mice (4–5 weeks old) were purchased from Hunan SJA Laboratory Animal Co., Ltd., and housed under pathogen-free conditions. Human osteosarcoma 143B cells (5×10^6) were subcutaneously injected into the right posterior flank of mice to establish a subcutaneous xenograft tumor. Mice were randomly allocated into different groups once the tumor volume reached 50 to 100 mm^3 and treated with the indicated drugs (DOX, 2 mg/kg, twice

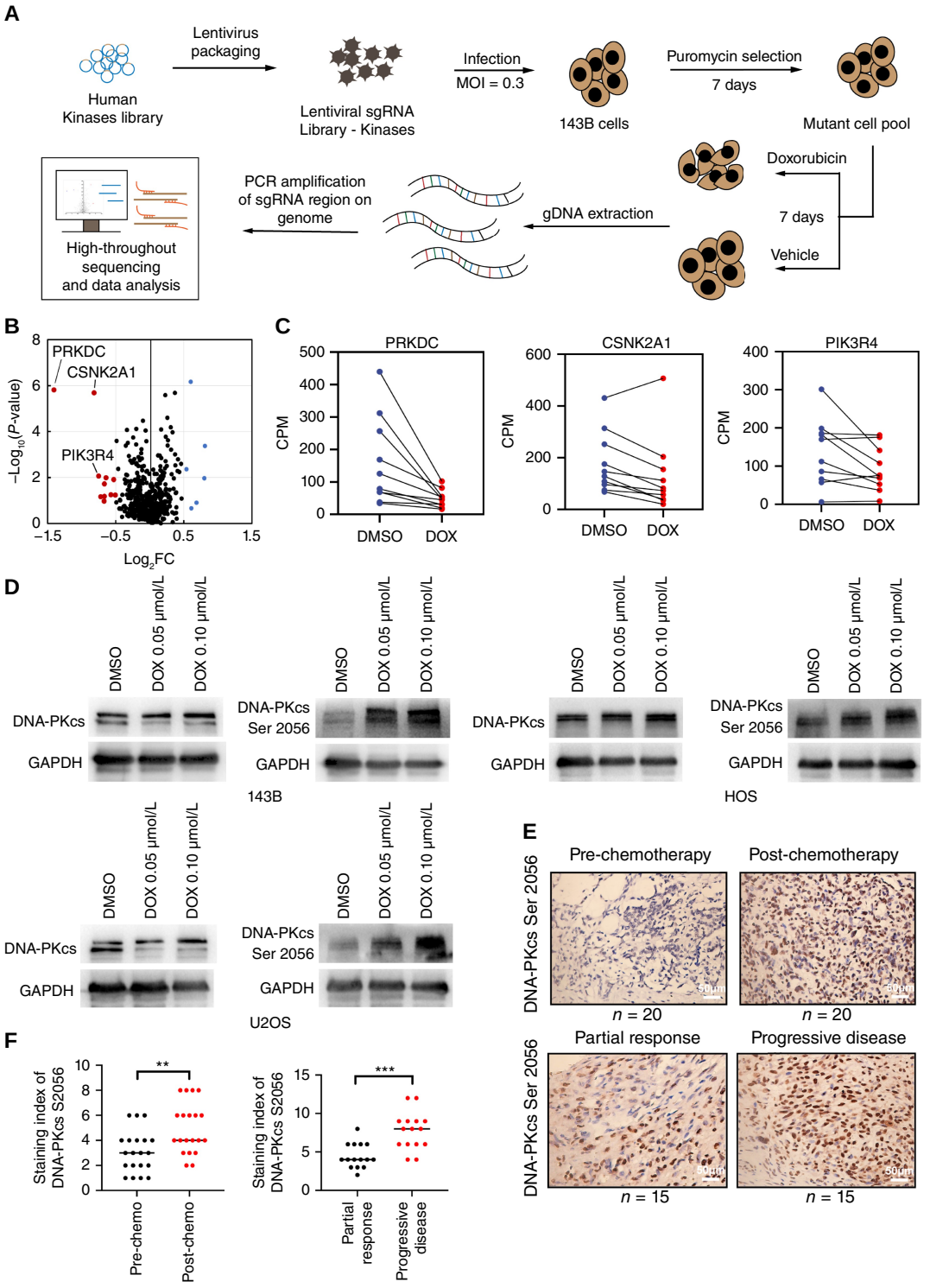

Figure 1.

CRISPR screen identifies PRKDC as a key determinant of DOX sensitivity in osteosarcoma. **A**, Workflow of the kinome-wide CRISPR screen in osteosarcoma. **B**, Volcano plot showing the enriched targeting genes of the screen. **C**, Comparisons of the CPM values of the top negatively enriched targeting genes between the DOX- and DMSO-treated groups. **D**, The 143B, HOS, and U2OS cells were treated with the indicated concentration of DOX for 72 hours, and the whole cell lysates were harvested for Western blot analysis. **E**, IHC analysis for the DNA-PKcs and DNA-PKcs S2056 expression in the prechemotherapy vs. postchemotherapy group or in the progressive disease vs. partial response group. **F**, Quantification of the IHC score in the indicated comparisons. Data are presented as the mean ± SD. **, $P < 0.01$; ***, $P < 0.001$.

a week, intraperitoneally; AZD7648, 70 mg/kg, once a day, orally). The tumor volume was calculated using the formula of $\pi/6 \times \text{length} \times \text{width}^2$. At the end of the experiments, the mice were euthanized, and the tumors were excised and weighed.

In vivo toxicity testing

To analyze the safety of drug combination treatment, BALB/c mice (4–5 weeks old) were randomly allocated into different groups and administered DOX, AZD7648, or their combination (DOX, 2 mg/kg, twice a week, intraperitoneally; AZD7648, 70 mg/kg, once a day, orally). At the end of treatment, the bone marrow, serum, liver, lung, heart, spleen, and kidney samples were collected for further analysis. Specifically, the bone marrow was digested into individual cells and stained for flow cytometry analysis. Serum markers of liver, kidney, and heart damage were detected using a relative assay kit (AST: #C010-2-1, Nanjing Jiancheng Bioengineering Institute, ALT: #C009-2-1, Nanjing Jiancheng Bioengineering Institute, LDH: #A020-2-2, Nanjing Jiancheng Bioengineering Institute, CK-MB: E-EL-M0355, Elabscience). Organic injury to the liver, lung, heart, spleen, and kidney was assessed by pathological analysis.

Organoid model

Patient-derived organoid models were derived from patients with osteosarcoma in our cancer center, following a previously described protocol (40). Briefly, fresh specimens were washed and fragmented into smaller sections. The minced tissues were further subjected to digestion. After filtration and centrifugation, the sediment was resuspended in a complete organoid culture medium. These cell clusters were further cultivated within a 96-well low-adsorption plate using a 3D-shaker system. The cell viability within organoids was assessed using the CellTiter-Glo 3D Cell Viability Assay Kit (Promega).

Drug–drug interaction assay

The Chou–Talalay combinatorial index (CI) was also used to evaluate drug synergies between DOX and AZD7648. The CI value was calculated using the following formula: $CI = DA/da + DB/db$, in which da and db are the IC_{50} doses of the single drugs, and DA and DB refer to the concentration of each drug in combination treatment in which the combination effect reached IC_{50}.

Statistical analysis

GraphPad Prism 9 was used for the statistical analyses. The experimental data are presented as the mean ± SD. Unpaired two-sided Student *t* test or one-way ANOVA was used for comparison between groups. Statistical significance was defined as *P*-values < 0.05.

Data Availability

The datasets used and/or analyzed during the current study are available from the corresponding authors on reasonable request. The data generated in this study are publicly available in Gene Expression Omnibus at GSE268415.

Results

CRISPR screen identifies PRKDC as a key determinant of DOX sensitivity in osteosarcoma

To explore the key kinases involved in DOX sensitivity in osteosarcoma, we conducted a kinome-wide CRISPR screen in 143B cells (**Fig. 1A**). We hypothesized that the knockout of a DOX-resistant gene could enhance the efficacy of DOX in tumor suppression. Under DOX treatment, cells carrying sgRNAs targeting core sensitive genes will be negatively selected. After selection, more than 500× coverage of cells was collected and sequenced, and 100% of the sgRNA sequences were retained in the DMSO-treated samples, which ensured the effectiveness of our screen. As a result, we identified six kinases that were significantly negatively enriched ($\log_2FC > 0.5$; $P < 0.05$) in DOX-treated cells compared with the vehicle control, including PRKDC, CSNK2A1, PIK3R4, MAPK3, ILK, and ICK (**Fig. 1B**), in which PRKDC was the most negatively selected gene, with all targeting sgRNAs decreased in the DOX treatment group (**Fig. 1C**). Thus, the loss of PRKDC could sensitize osteosarcoma cells to DOX treatment.

We next detected the level of DNA-PKcs protein and DNA-PKcs Ser2056 phosphorylation to explore the response of PRKDC to DOX treatment. We demonstrated an elevated expression of DNA-PKcs Ser2056 phosphorylation, but not DNA-PKcs protein (**Fig. 1D**), indicating that DOX treatment activated PRKDC in osteosarcoma. We also detected the level of DNA-PKcs Ser2056 phosphorylation in paired pre- and post-chemotherapy osteosarcoma tissues by IHC, and the results showed that DNA-PKcs Ser2056 phosphorylation was significantly increased in post-chemotherapy tissues (**Fig. 1E** and **F**). Meanwhile, we assessed the chemotherapeutic outcome of patients with osteosarcoma from our cancer center according to RECIST 1.1. The DNA-PKcs Ser2056 phosphorylation level was evaluated in tumor tissues from 15 pairs of patients with a status of progressive disease or partial response. We found that DNA-PKcs Ser2056 was upregulated in tissues from the progressive disease group (**Fig. 1E** and **F**). These findings suggest that PRKDC plays a critical role in the response to DOX treatment and may promote the development of DOX resistance.

PRKDC plays a key role in modulating the sensitivity of osteosarcoma to DOX

To validate the impact of PRKDC on DOX sensitivity in osteosarcoma, we constructed a sgRNA vector targeting PRKDC and generated stable PRKDC knockout cells. Western blotting confirmed that both sgRNAs were able to eliminate the expression of DNA-PKcs protein in the 143B, HOS, U2OS, and MG63 cell lines (**Fig. 2A**). The PRKDC knockout showed no obvious impact on cell growth (Supplementary Fig. S1A), whereas PRKDC knockout significantly suppressed cell proliferation and induced cell apoptosis under the treatment of DOX (**Fig. 2A–D**; Supplementary Fig. S1B). Hence, the PRKDC knockout could significantly enhance the sensitivity of osteosarcoma to DOX treatment. We also explored the sensitivity of PRKDC knockout cells to other chemotherapy drugs for osteosarcoma, including cisplatin, methotrexate, and sorafenib. We found that the PRKDC knockout did not affect the sensitivity of osteosarcoma to these drugs (Supplementary Fig. S1C), indicating that the PRKDC knockout specifically increased the DOX sensitivity. Subsequently, we examined other chemotherapy drugs that induce DNA double-strand breaks, including etoposide and teniposide. The results showed that the PRKDC knockout also significantly increased the sensitivity of osteosarcoma to them (Supplementary Fig. S1D).

We next confirmed these observations in an *in vivo* model. To this end, 143B cells with or without PRKDC knockout were inoculated in the right posterior flank of the BALB/c nude mice. When the tumor volume reached 50 to 100 mm^3, the mice were treated with DOX or vehicle control for 14 days. The result confirmed that the depletion of PRKDC significantly increased the sensitivity of the osteosarcoma model mice to DOX treatment (**Fig. 2E–H**).

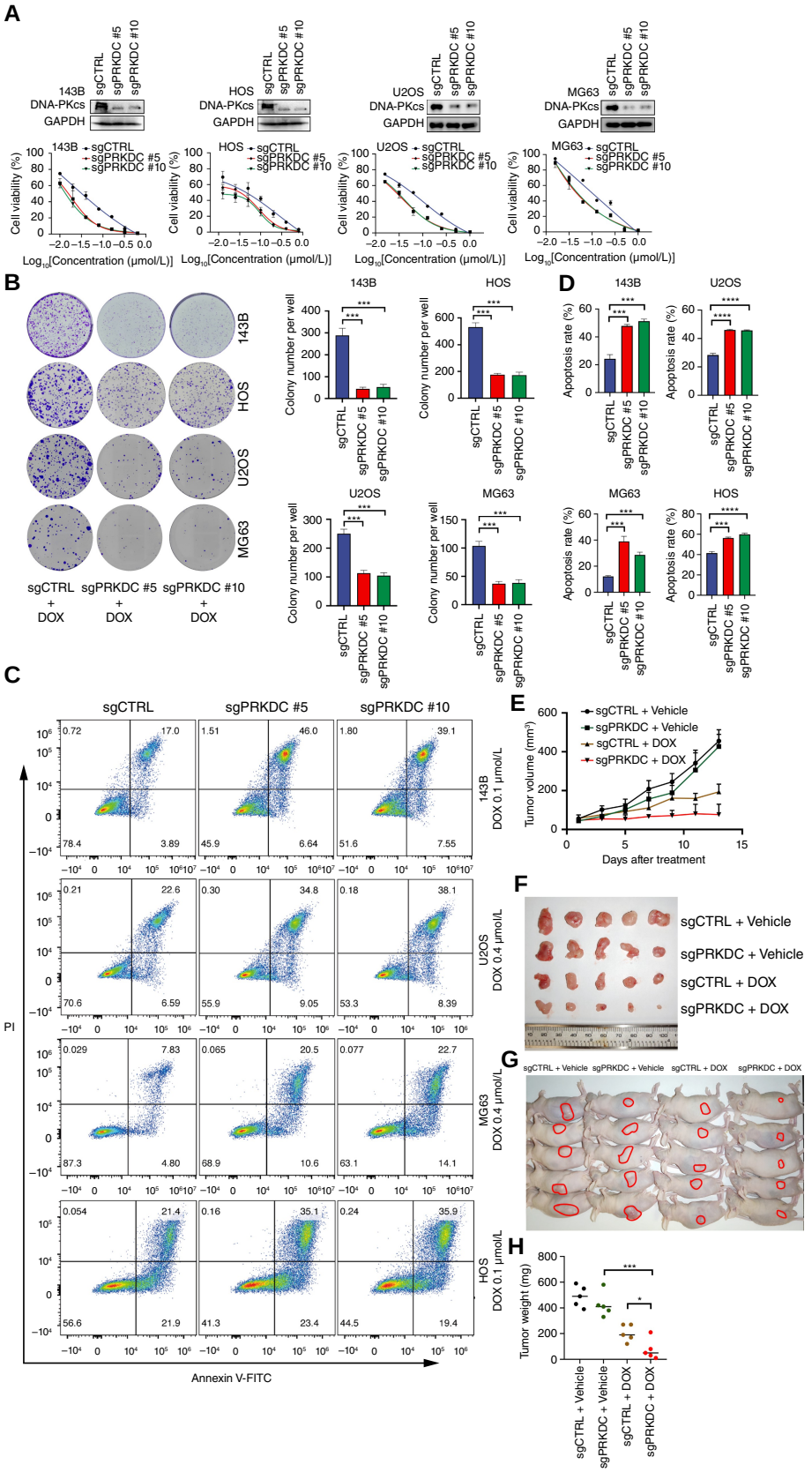

Figure 2.

PRKDC plays a key role in modulating the sensitivity of osteosarcoma to DOX. **A**, PRKDC was knocked out in the 143B, HOS, U2OS, and MG63 cells using the CRISPR/Cas9 gene editing system. These cells were treated with a serial dose of DOX for 48 hours before subjecting them to the CCK-8 assay. **B–D**, The 143B, HOS, U2OS, and MG63 cells were transfected with the indicated constructs for 48 hours. After puromycin selection, these cells were subjected to colony formation assay (3.25 nmol/L DOX for 143B and HOS; 6.25 nmol/L for U2OS and MG63) and Annexin V-FITC/PI assay with the indicated treatment. Data are presented as the mean ± SD with three replicates. **E–H**, The 143B cells were transfected with the indicated constructs for 48 hours. After puromycin selection, these cells were subcutaneously injected into the nude mice before treating the mice with or without DOX (2 mg/kg, twice a week, intraperitoneally). Tumor growth curve (**E**), tumor images (**F**), mouse images (**G**), and tumor mass (**H**) are shown. Data are presented as the mean ± SD with five replicates. *, $P < 0.05$; ***, $P < 0.001$; ****, $P < 0.0001$.

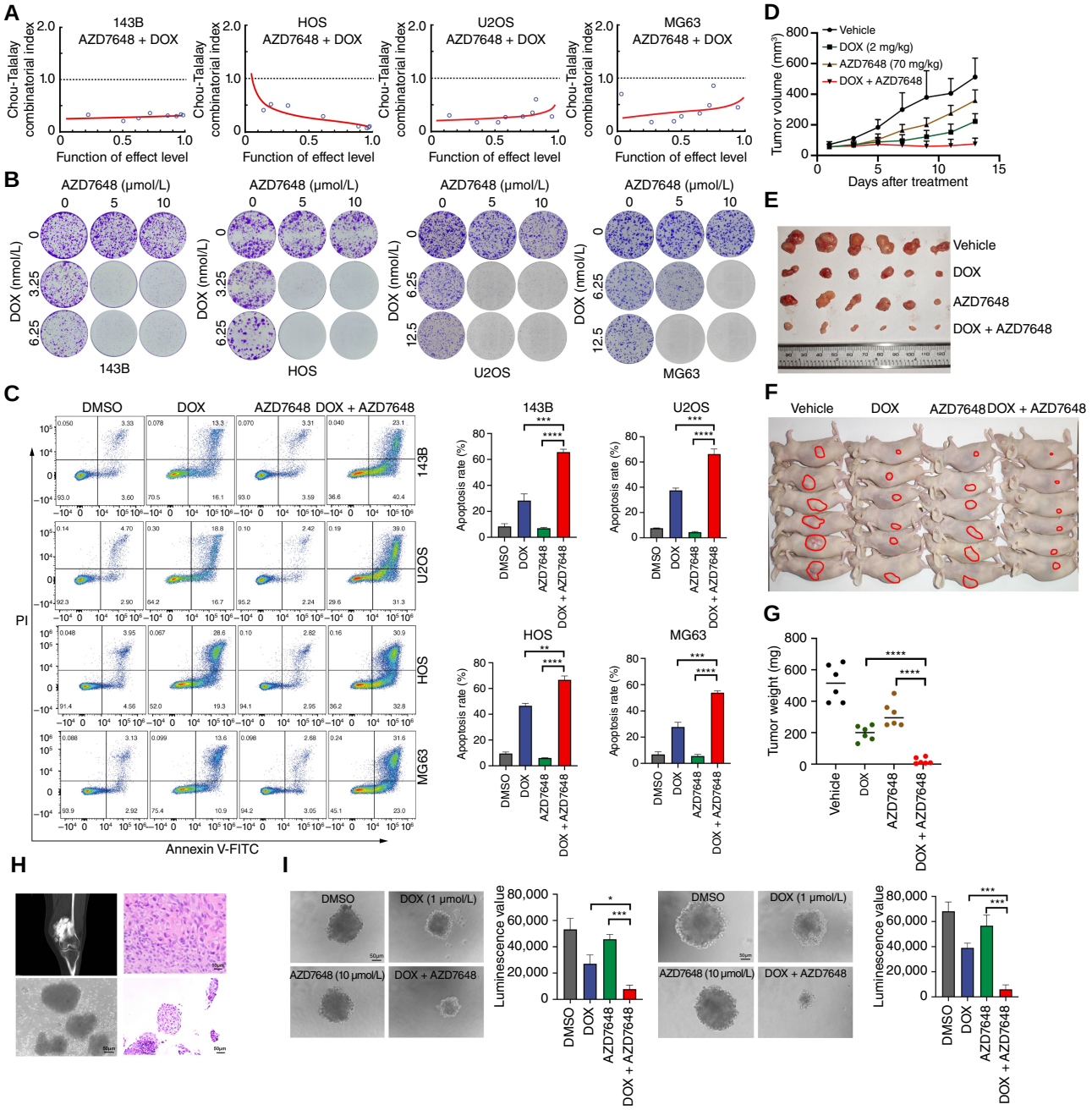

Figure 3.

PRKDC inhibitor AZD7648 synergized with DOX in the suppression of osteosarcoma. **A**, 143B, HOS, U2OS, and MG63 cells were treated with the indicated drugs or drug combinations for 48 hours before subjecting them to the CCK-8 assay. DOX was 2-fold diluted starting from 0.8 μmol/L, while AZD7648 was 2-fold diluted starting from 80 μmol/L for the 143B and HOS cells. For the U2OS and MG63 cells, DOX was 2-fold diluted starting from 3.2 μmol/L, and AZD7648 was 2-fold diluted starting from 50 μmol/L. The Chou–Talalay combinatorial index (CI) was used to evaluate the synergistic effect of the combination treatment. **B**, Colony formation assay of the 143B, HOS, U2OS, and MG63 cells with the indicated treatment. **C**, The 143B, HOS, U2OS, and MG63 cells were treated with the indicated drugs or drug combinations for 48 hours (0.1 μmol/L DOX; 10 μmol/L AZD7648) before subjecting them to the Annexin V-FITC/PI assay. Data are presented as the mean ± SD with three replicates. **D–G**, 143B cells were subcutaneously injected into the nude mice and treated with the indicated drugs or drug combination (DOX, 2 mg/kg, twice a week, intraperitoneally; AZD7648, 70 mg/kg, once a day, orally). Tumor growth curve (**D**), tumor images (**E**), mouse images (**F**), and tumor mass (**G**) are shown. Data are presented as the mean ± SD with six replicates. **H** and **I**, Osteosarcoma organoids were derived from two patients. The organoids were treated with the indicated drugs or drug combination. After 48 hours of incubation, the viability of the organoids was determined using the CellTiter-Glo 3D Cell Viability Assay. Data are presented as the mean ± SD with three replicates. *, $P < 0.05$; **, $P < 0.01$; ***, $P < 0.001$; ****, $P < 0.0001$.

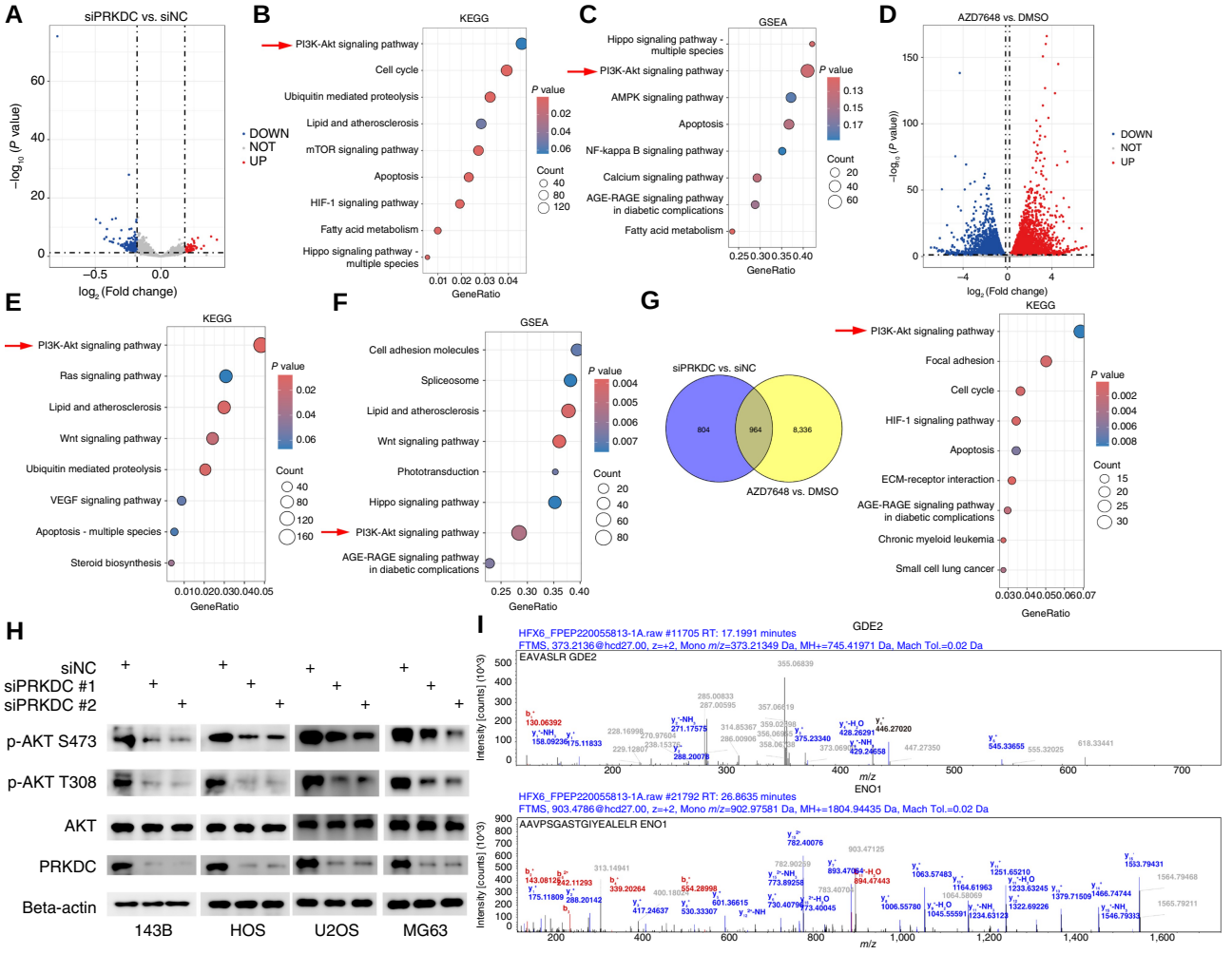

Figure 4.

PRKDC binds with GDE2 to activate the PI3K-AKT signaling pathway and regulate DOX sensitivity in osteosarcoma. **A–C,** Volcano plot (**A**), KEGG enrichment analysis (**B**), and GSEA (**C**) of RNA-seq after knockdown of PRKDC in HOS cells. **D–F,** Volcano plot (**D**), KEGG enrichment analysis (**E**), and GSEA (**F**) of RNA-seq after treatment with PRKDC inhibitors (AZD7648, 150 μmol/L) in HOS cells. **G**, Venn diagram showing the numbers of deferentially expressed genes and GSEA of common differential genes in the siPRKDC vs. siNC group and the AZD7648 vs. DMSO group. **H**, The 143B, HOS, U2OS, and MG63 cells were transfected with siNC, siPRKDC #1, or siPRKDC #2 for 48 hours, before harvesting for Wwestern blotting. **I**, The whole cell lysate of HOS cells was harvested for immunoprecipitation assay using anti-PRKDC antibody and subjected to LC–MS/MS analysis. (*Continued on the following page.*)

In addition, the group with the PRKDC knockout and DOX treatment showed significantly reduced Ki-67-positive cells and increased cleaved caspase-3-positive cells in osteosarcoma tissues compared with the other groups (Supplementary Fig. S1E). These findings suggest that PRKDC is an important driver of DOX sensitivity in osteosarcoma.

PRKDC inhibitor AZD7648 synergizes with DOX in the suppression of osteosarcoma

AZD7648 is a small molecule inhibitor specific for PRKDC inhibition. We next tested whether AZD7648 could work synergistically with DOX in the suppression of osteosarcoma. The Chou–Talalay method was used to evaluate the synergistic effect. The results revealed that AZD7648 and DOX synergistically inhibited the growth of four osteosarcoma cell lines at multiple concentrations (**Fig. 3A**), indicating that AZD7648 is a sensitizer for DOX in osteosarcoma. Similarly, we found that AZD7648 treatment did not significantly increase the sensitivity of osteosarcoma cells to cisplatin and methotrexate (Supplementary Fig. S2A and S2B). Moreover, the combination treatment of AZD7648 and DOX significantly impeded cell proliferation and induced cell apoptosis compared with single drug treatment (**Fig. 3B** and **C**; Supplementary Fig. S2C).

Next, we performed *in vivo* validation in a subcutaneous xenograft mouse model. When the tumor reached 50 to 100 mm^3, the mice were randomly divided into four groups and treated with vehicle, DOX, AZD7648, or the combination of DOX and AZD7648. DOX treatment alone suppressed tumor growth, whereas the combination of DOX and AZD7648 completely halted osteosarcoma growth *in vivo* (**Fig. 3D–G**). The

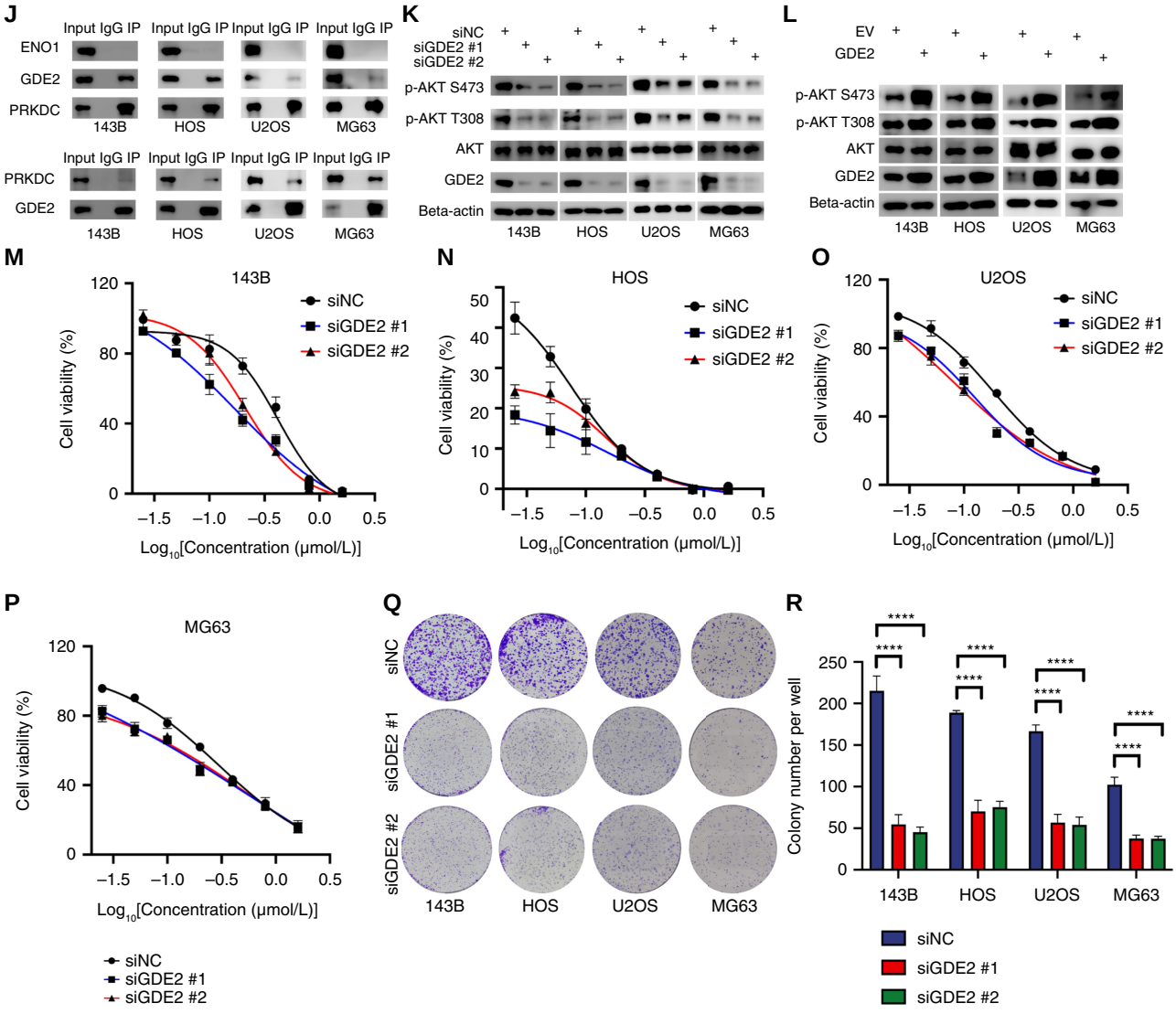

Figure 4.

(*Continued.*) **J**, The whole cell lysates of the 143B, HOS, U2OS, and MG63 cells were harvested for the co-IP assay. **K**, The 143B, HOS, U2OS, and MG63 cells were transfected with siNC, siGDE2 #1, or siGDE2 #2 for 48 hours, before harvesting for Western blotting. **L**, The 143B, HOS, U2OS, and MG63 cells were transfected with the indicated EV or GDE2 overexpression constructs for 48 hours, before harvesting for Western blotting. **M–P,** The 143B, HOS, U2OS, and MG63 cells were transfected with the indicated siNC, siGDE2 #1, or siGDE2 #2 for 48 hours. These cells were treated with a serial dose of DOX for 48 hours and subjected to the CCK-8 assay. **Q–R,** The effects of GDE2 knockdown on cell growth under DOX treatment were analyzed by colony formation (3.25 nmol/L DOX for 143B and HOS cells, 6.25 nmol/L DOX for U2OS and MG63 cells). Data are presented as the mean ± SD with three replicates. ****, $P < 0.0001$.

tumor tissues from the combination treatment group showed a significantly decreased expression of Ki-67 and increased levels of cleaved caspase 3 (Supplementary Fig. S2D). To further validate the efficacy of this combination, we established two cases of osteosarcoma organoids (**Fig. 3H**), which were treated with vehicle, DOX alone, AZD7648 alone, or a combination of DOX and AZD7648. Remarkably, the combination therapy demonstrated significant inhibition of the growth of osteosarcoma organoids (**Fig. 3I**). We next explored the impact of PRKDC inhibition on DOX across various solid tumors, including lung, liver, and prostate cancers. Intriguingly, our findings revealed that PRKDC inhibition markedly heightened the responsiveness of these tumors to DOX (Supplementary Fig. S3A–S3C). Notably, the combined administration of DOX and AZD7648 exhibited synergistic suppression of these tumors (Supplementary Fig. S3D–S3F).

To assess the safety profile of the DOX and AZD7648 combination, we conducted *in vivo* toxicity tests in BALB/c mice. The mice were randomly divided into four groups and subjected to corresponding drug treatments for 14 days. At the end of the experiment, the bone marrow, blood plasma, heart, liver, kidney, lung, and spleen samples were collected for further analysis (Supplementary Fig. S4A). The results revealed that DOX treatment alone induced bone marrow suppression (Supplementary Fig. S4B),

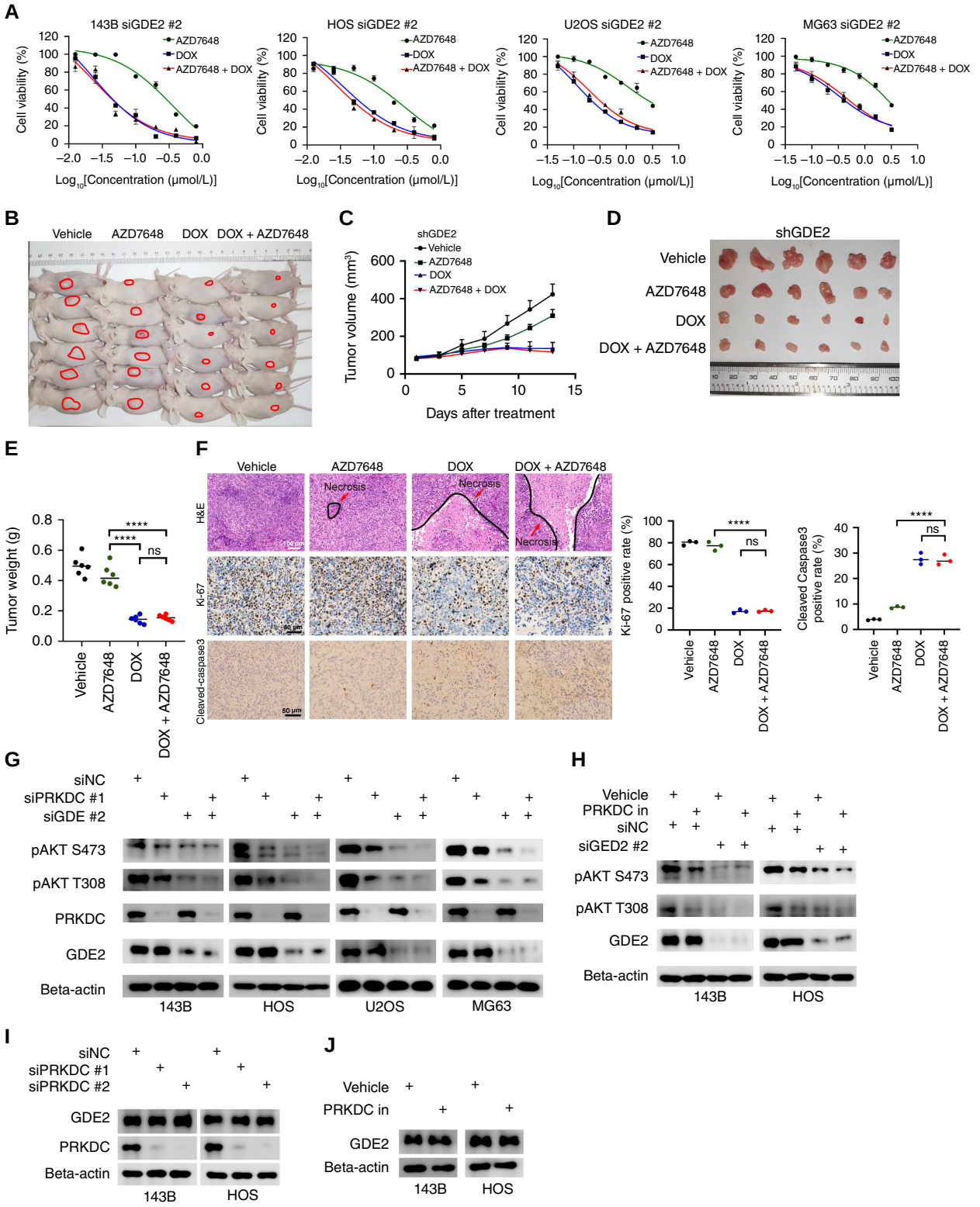

Figure 5.

GDE2 is responsible for PRKDC-mediated DOX sensitivity in osteosarcoma. **A,** The 143B, HOS, U2OS, and MG63 cells were transfected with siGDE2 #2 for 48 hours. These cells were treated with the indicated drugs or drug combination for 48 hours and subjected to the CCK-8 assay. DOX was 2-fold diluted starting from 0.8 μmol/L, and AZD7648 was 2-fold diluted starting from 80 μmol/L for the 143B and HOS cells. For the U2OS and (*Continued on the following page.*)

nephrotoxicity (Supplementary Fig. S4C), and cardiotoxicity (Supplementary Fig. S5A), whereas it had no significant impact on the spleen (Supplementary Fig. S5B), lung (Supplementary Fig. S5C), and liver (Supplementary Fig. S5D). Importantly, compared with DOX treatment alone, the combination of DOX and AZD7648 did not remarkably exacerbate these toxic effects. Taken together, these findings demonstrate that the combination treatment achieved both satisfactory efficacy and safety.

PRKDC binds with GDE2 to activate the PI3K-AKT signaling pathway and regulate DOX sensitivity in osteosarcoma

To further reveal the underlying mechanisms of PRKDC-mediated DOX sensitivity in osteosarcoma, HOS cells were transfected with PRKDC siRNAs or treated with AZD7648, and then subjected to transcriptome analysis. The Kyoto Encyclopedia of Genes and Genomes (KEGG) enrichment analysis and the gene set enrichment analysis indicated that both siRNA and AZD7648 treatment downregulated the PI3K/AKT signaling pathway (**Fig. 4A–F**). We also identified 964 common differentially expressed genes in both the PRKDC-knockdown and AZD7648-treated cells (**Fig. 4G**) and confirmed that they were also enriched in the PI3K/AKT pathway (**Fig. 4G**). Consistent with the transcriptome analysis, Western blot analysis revealed that the AKT phosphorylation levels were decreased in the PRKDC-knockdown cells compared with the control (**Fig. 4H**).

To elucidate the mechanism by which PRKDC regulates the PI3K/AKT pathway, the PRKDC interactors were purified using IP and identified using LC–MS/MS. As a result, we found several PRKDC-associated proteins, among which, GDE2 and ENO1 were the top two potential PRKDC interactors (**Fig. 4I**). However, coimmunoprecipitation (co-IP) analysis in the 143B, HOS, U2OS, and MG63 cells confirmed that only GDE2 binds to the PRKDC protein (**Fig. 4J**). Echoed with PRKDC regulation, the GDE2 knockdown reduced the AKT phosphorylation levels in osteosarcoma cells (**Fig. 4K**), whereas the GDE2 overexpression elevated AKT phosphorylation levels (**Fig. 4L**). Knockdown of GDE2 alone had no obvious impact on osteosarcoma cell proliferation and apoptosis (Supplementary Fig. S6A and S6B), but significantly restrained the growth of osteosarcoma cells under the treatment of DOX (**Fig. 4M–R**). These findings demonstrate that PRKDC could regulate DOX sensitivity in osteosarcoma by binding with GDE2 to activate the PI3K/AKT pathway.

GDE2 is responsible for PRKDC-mediated DOX sensitivity in osteosarcoma

To assess whether GDE2 was responsible for PRKDC-mediated DOX sensitivity, we treated GDE2-knockdown cells with AZD7648, DOX, or their combination. We found that GDE2 knockdown eliminated the superior efficacy of combination treatment compared with DOX treatment alone (**Fig. 5A**). The results of the *in vivo* experiment showed that the therapeutic effect of DOX was not impacted by AZD7648 in GDE2-knockdown tumors (**Fig. 5B–F**). We further demonstrated that GDE2 knockdown diminished the effect of PRKDC on the alterations in AKT phosphorylation (**Fig. 5G**). Similarly, the effect of the PRKDC inhibitor AZD7648 on AKT phosphorylation was also removed by GDE2 knockdown (**Fig. 5H**). Taken together, these data suggest that the effect of PRKDC on DOX sensitivity and AKT phosphorylation is mediated by GDE2. However, the protein level of GDE2 was not significantly affected by PRKDC knockdown or AZD7648 treatment (**Fig. 5I** and **J**), indicating that PRKDC recruited but did not regulate the stability of GDE2.

PRKDC recruits GDE2 to stabilize GNAS and activates the PI3K/AKT signaling pathway in osteosarcoma

We further investigated the specific mechanism by which GDE2 regulates the PI3K/AKT pathway. We compared the level of GDE2-binding protein between cells with and without PRKDC knockdown. The co-IP and LC–MS/MS analyses revealed that the binding of GNAS to GDE2 in PRKDC-knockdown cells was significantly reduced compared with that in the relative control (**Fig. 6A**). Previous studies reported that the activated mutation of GNAS was associated with the progression of osteosarcoma (41, 42), and that the overexpression of GNAS promoted activation of the PI3K/AKT pathway (43).

The co-IP assay confirmed that GNAS and GDE2 interacted with each other in osteosarcoma cells (**Fig. 6B**). Therefore, we hypothesized that GDE2 binds with GNAS to modulate the PI3K/AKT pathway. The knockdown of GDE2 significantly decreased the expression of the GNAS protein but did not significantly alter its mRNA expression (**Fig. 6C** and **D**). In addition, treatment with AZD7648 or PRKDC knockdown downregulated the protein, but not the mRNA level of GNAS in osteosarcoma cells (**Fig. 6E–G**). More importantly, we demonstrated that GDE2 knockdown eradicated the effect of PRKDC knockdown or AZD7648 treatment on the GNAS protein expression (**Fig. 6H** and **I**). The co-IP assay using the anti-GDE2 antibody further demonstrated that PRKDC knockdown or AZD7648 treatment significantly reduced the binding of GNAS to GDE2 (**Fig. 6J** and **K**). These data indicated that PRKDC could stabilize the GNAS protein by recruiting GDE2.

In addition, GNAS knockdown remarkably reduced AKT phosphorylation in osteosarcoma cells (**Fig. 6L**) and eliminated the effect of GDE2 knockdown on AKT phosphorylation (**Fig. 6M**). Consistently, the effect of PRKDC knockdown or AZD7648 treatment on AKT phosphorylation was also diminished by GNAS knockdown (**Fig. 6N** and **O**). These findings suggest that PRKDC regulates AKT phosphorylation and DOX sensitivity by recruiting GDE2 to stabilize the GNAS expression. As evidence has shown that AKT activation directly participates in DNA damage response and repair, we

(*Continued*.) MG63 cells, DOX was 2-fold diluted starting from 3.2 μmol/L and AZD7648 was 2-fold diluted starting from 50 μmol/L. The *x*-axis indicates the concentration of DOX. **B–E,** The 143B cells were transfected with the indicated constructs for 48 hours. After puromycin selection, these cells were subcutaneously injected into nude mice, which were then treated with the indicated drugs or drug combination (DOX, 2 mg/kg, twice a week, intraperitoneally; AZD7648, 70 mg/kg, once a day, orally). The mouse images (**B**), tumor growth curve (**C**), tumor images (**D**), and tumor mass (**E**) were assessed. **F,** Hematoxylin and eosin (H&E), Ki-67 IHC, and cleaved caspase-3 IHC staining of tumors with indicated treatment. Data are presented as the mean ± SD with three replicates. **G,** The 143B, HOS, U2OS, and MG63 cells were transfected with the indicated siNC, siPRKDC #1, siGDE2 #2, or siPRKDC #1 + siGDE2 #2 for 48 hours before harvesting the cells for Western blotting. **H,** The 143B and HOS cells were transfected with the indicated siNC or siGDE2 #2 for 48 hours and treated with or without AZD7648 (150 μmol/L) before harvesting the cells for Western blotting. **I,** The 143B and HOS cells were transfected with the indicated siNC, siPRKDC #1, or siPRKDC #2 for 48 hours, before harvesting the cells for Western blotting of the indicated proteins. **J,** The 143B and HOS cells were treated with AZD7648 (150 μmol/L for 24 hours) before harvesting the cells for Western blotting. ns, not significant; ****, $P < 0.0001$.

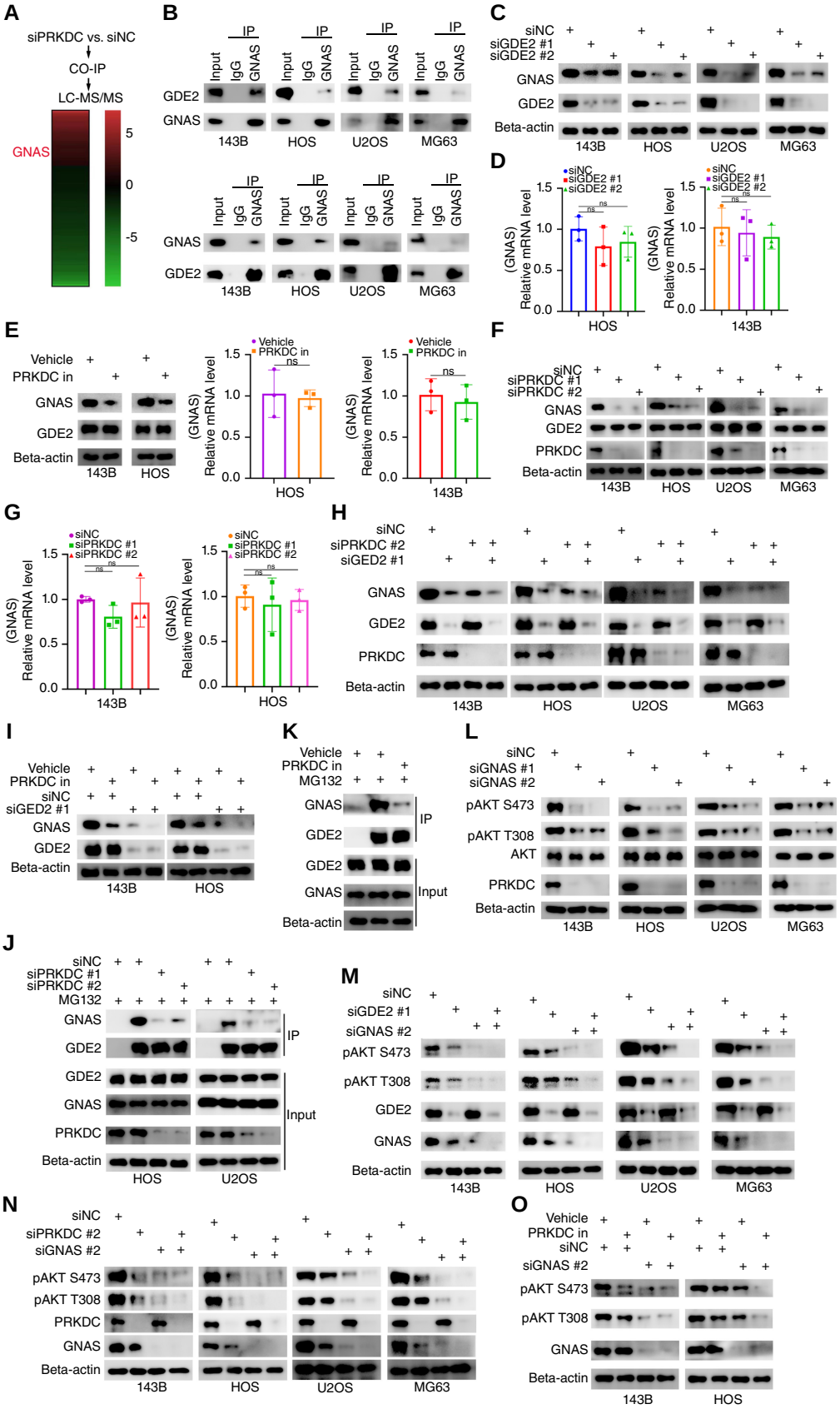
A
siPRKDC vs. siNC
CO-IP
LC-MS/MS
GNAS
5
0
-5
B
IP
Input
IgG
GNAS
GDE2
143B
HOS
U2OS
MG63
C
siNC
siGDE2 #1
siGDE2 #2
GNAS
GDE2
Beta-actin
D
(GNAS) Relative mRNA level
ns
E
Vehicle
PRKDC in
F
siPRKDC #1
siPRKDC #2
PRKDC
G
H
siGED2 #1
I
K
MG132
IP
Input
L
siGNAS #1
siGNAS #2
pAKT S473
pAKT T308
AKT
J
M
N
O

sought to investigate whether AKT regulates DNA damage in osteosarcoma cells (44). To this end, we analyzed the levels of DNA damage in osteosarcoma cells with AKT inhibition. The results indicated that AKT inhibition significantly increased DOX-induced DNA damage (Supplementary Fig. S6C), demonstrating that the PRKDC/GDE2/GNAS axis regulates DOX sensitivity by modulating the AKT-mediated DNA damage response.

A previous study reported that PRKDC regulates the nonhomologous end-joining (NHEJ) process to mediate DNA repair (45). Therefore, we investigated whether impaired NHEJ repair due to PRKDC inhibition contributes to increased DOX sensitivity in osteosarcoma. Our findings revealed that the GDE2/GNAS overexpression largely attenuated the effect of PRKDC inhibition on DOX sensitivity, suggesting that PRKDC primarily modulates DOX sensitivity through the GDE2/GNAS axis in osteosarcoma (Supplementary Fig. S7A and S7B). We also examined the interplay of PRKDC/GDE2/GNAS with the BCL2 family, which may account for the increase in DOX-induced cell death. Interestingly, our results indicated that the knockdown of PRKDC/GDE2/GNAS had no discernible impact on the expression of BCL-2 and BAX (Supplementary Fig. S7C–S7E).

Discussion

Despite the advances in tumor biology over the past decades, the therapeutic method for osteosarcoma remains limited, especially for patients with drug resistance or metastasis. Kinases are often activated in cancers and contribute to tumor progression and drug resistance (46, 47). In this study, we conducted a kinome-wide CRISPR screen and identified PRKDC as a critical determinant of DOX sensitivity in osteosarcoma. The knockout of PRKDC remarkably increased the sensitivity of osteosarcoma to DOX. Previous studies have also reported that inhibition of PRKDC enhances the efficacy of DOX in cancer treatment. Fok and colleagues found that the PRKDC inhibitor AZD7648 increased DOX sensitivity in breast cancer (23). Similarly, the PRKDC inhibitor NU7441 sensitized breast cancer cells to radiation and DOX therapy (24). However, these studies did not illustrate the underlying mechanisms of PRKDC-mediated DOX sensitivity.

Through a transcriptome analysis, we observed that the PI3K/AKT pathway was downregulated upon PRKDC knockdown or AZD7648 treatment. Consistently, previous findings have also demonstrated that PRKDC could regulate the activation of the PI3K/AKT pathway (48). Inhibition of the PI3K/AKT signaling pathway has been shown to increase DOX sensitivity in breast cancer (49). Thus, we hypothesized that PRKDC-mediated DOX sensitivity was attributed to its ability to regulate the PI3K/AKT signaling pathway. We further studied the molecular mechanisms that collectively control the PI3K/AKT pathway and the sensitivity of osteosarcoma to DOX. The results showed that PRKDC could recruit GDE2 in an expression-independent manner. GDE2 is a chemoresistance-related gene that was previously reported to regulate 5-Fu resistance in colorectal cancer and confer cisplatin resistance in nasopharyngeal carcinoma (28, 29). We found that GDE2 knockdown improved DOX sensitivity in osteosarcoma by regulating the AKT pathway activation. More specifically, GDE2 activates AKT by binding to GNAS and stabilizes its expression. Collectively, these findings expound on a novel mechanism for PRKDC-mediated DOX sensitivity.

While the involvement of PRKDC and AKT in DOX resistance has been reported in other tumors, the detailed mechanistic axis remains incompletely elucidated, particularly in osteosarcoma, in which relevant studies are lacking. Significantly, our study revealed that in osteosarcoma, PRKDC predominantly affected DOX sensitivity through modulation of the GDE2/GNAS/AKT axis, rather than by directly regulating NHEJ repair (50). This discovery offers novel insights into the influence of PRKDC on DOX sensitivity, which will assist with the development of related therapeutics in the future.

Drug combination constitutes a fundamental approach for osteosarcoma therapy because it can overcome compensatory mechanisms and increase therapeutic efficacy (51, 52). We systematically explored drug combination treatment strategies for osteosarcoma in our previous study (53). Herein, we demonstrated that knockout of PRKDC obviously increased DOX sensitivity and that the PRKDC inhibitor AZD7648 could significantly synergize with DOX in the suppression of osteosarcoma growth. A Phase I/IIa clinical trial is underway to evaluate the therapeutic efficacy of the combination of AZD7648 and pegylated liposomal DOX in patients with advanced cancers (NCT03907969). We propose that the combination of AZD7648 and DOX represents a strategy for osteosarcoma therapy with excellent potential, although clinical trials are still needed to evaluate its effectiveness and safety. In addition, there is currently no inhibitor for GDE2 and GNAS. Identifying these inhibitors

Figure 6.

PRKDC recruits GDE2 to stabilize GNAS and activates the PI3K-AKT signaling pathway in osteosarcoma. **A,** The HOS cells were transfected with the indicated siNC or siPRKDC #2 for 48 hours, before harvesting the cells for the LC–MS/MS analysis. **B,** whole cell lysates of 143B, HOS, U2OS, and MG63 cells were harvested for co-IP assay. **C,** The 143B, HOS, U2OS, and MG63 cells were transfected with siNC, siGDE2 #1, or siGDE2 #2 for 48 hours before harvesting the cells for Western blotting. **D,** The 143B and HOS cells were transfected with the indicated siRNAs for 48 hours before harvesting the cells for qRT–PCR. Data are presented as the mean ± SD of three independent experiments. **E,** The 143B and HOS cells were treated with AZD7648 (150 μmol/L) for 24 hours, before harvesting the cells for Western blotting and qRT–PCR. **F,** The 143B, HOS, U2OS, and MG63 cells were transfected with siNC, siPRKDC #1, or siPRKDC #2 for 48 hours, before harvesting the cells for Western blotting. **G,** The 143B and HOS cells were transfected with the indicated siRNAs for 48 hours, before harvesting the cells for qRT–PCR. Data are presented as the mean ± SD of three independent experiments. **H,** The 143B, HOS, U2OS, and MG63 cells were transfected with the indicated siNC, siPRKDC #2, siGDE2 #1, or siPRKDC #2 + siGDE2 #1 for 48 hours before harvesting the cells for Western blotting. **I,** The 143B and HOS cells were transfected with the indicated siNC or siGDE2 #1 for 48 hours and treated with or without AZD7648 (150 μmol/L) for 24 hours, before harvesting the cells for Western blotting. **J,** The HOS and U2OS cells were transfected with the indicated siNC, siPRKDC #1, or siPRKDC #2 for 48 hours and treated with a proteasome inhibitor (MG132, 2 μmol/L) for 24 hours, before harvesting the cells for the co-IP assay. **K,** The HOS cells were treated with AZD7648 (150 μmol/L) and MG132 (2 μmol/L) for 24 hours, before harvesting the cells for the co-IP assay. **L,** The 143B, HOS, U2OS, and MG63 cells were transfected with siNC, siGNAS #1, or siGNAS #2 for 48 hours, before harvesting the cells for Western blotting. **M,** The 143B, HOS, U2OS, and MG63 cells were transfected with siNC, siGDE2 #1, siGNAS #2, or siGDE2 #1 + siGNAS #2 for 48 hours, before harvesting the cells for Western blotting. **N,** The 143B, HOS, U2OS, and MG63 cells were transfected with siNC, siPRKDC #2, siGNAS #2, or siPRKDC #2 + siGNAS #2 for 48 hours, before harvesting the cells for Western blotting. **O,** The 143B and HOS cells were transfected with the indicated siNC or siGNAS #2 for 48 hours and treated with or without AZD7648 (150 μmol/L) for 24 hours, before harvesting the cells for Western blotting. ns, not significant.

through high-throughput screening may provide new therapeutic alternatives for unmet clinical applications. However, this may present a challenge because GDE2 and GNAS are ubiquitous and may not be feasible therapeutic targets.

In summary, our results suggest the critical role of PRKDC in DOX sensitivity of osteosarcoma. Mechanistically, PRKDC could recruit GDE2 to stabilize the GNAS expression and activate the PI3K/AKT signaling pathway. The PRKDC/GDE2/GNAS/AKT axis could serve as a potential target for enhancing DOX sensitivity in osteosarcoma, and the corresponding combinational therapy strategies are well worth developing.

Authors' Disclosures

No disclosures were reported.

Authors' Contributions

W. Zhang: Conceptualization, data curation, formal analysis, validation, investigation, visualization, methodology, and writing–review and editing. **W. Li:** Conceptualization, data curation, formal analysis, validation, investigation, visualization, methodology, and writing–review and editing. **C. Yin:** Resources, investigation, and methodology. **C. Feng:** Resources, investigation, and methodology. **B. Liu:** Investigation and methodology. **H. Xu:** Investigation and methodology. **X. Jin:** Conceptualization, data curation, supervision, investigation, and writing–review and editing. **C. Tu:** Conceptualization, resources, data curation, supervision, funding acquisition, project administration, and writing–review and editing. **Z. Li:** Conceptualization, resources, data curation, formal analysis, supervision, funding acquisition, project administration, and writing–review and editing.

Acknowledgments

This work was supported by the National Natural Foundation of China (grant no. 82272664 to C. Tu; grant no. 82172500 to Z. Li), National Key Research and Development Program of China (grant no. 2023YFC2507603 to Z. Li), Science and Technology Innovation Program of Hunan Province (grant no. 2023RC3085 to C. Tu), Hunan Provincial Natural Science Foundation of China (grant no. 2022JJ30843 to C. Tu), Science and Technology Development Fund Guided by Central Government (grant no. 2021Szvup169 to Z. Li), Hunan Provincial Administration of Traditional Chinese Medicine Project (grant no. D2022117 to C. Tu), Scientific Research Program of Hunan Provincial Health Commission (grant no. B202304077077 to C. Tu), and Hunan Provincial Health High-level Talent Scientific Research Project (grant no. R2023054 to C. Tu). We thank LetPub (www.letpub.com) for its linguistic assistance during the preparation of this manuscript.

Note

Supplementary data for this article are available at Cancer Research Online (http://cancerres.aacrjournals.org/).

Received January 17, 2024; revised May 13, 2024; accepted June 14, 2024; published first June 20, 2024.

References

1. Meltzer PS, Helman LJ. New horizons in the treatment of osteosarcoma. N Engl J Med 2021;385:2066–76.
2. Wen Y, Tang F, Tu C, Hornicek F, Duan Z, Min L. Immune checkpoints in osteosarcoma: recent advances and therapeutic potential. Cancer Lett 2022;547:215887.
3. Tian H, Cao J, Li B, Nice EC, Mao H, Zhang Y, et al. Managing the immune microenvironment of osteosarcoma: the outlook for osteosarcoma treatment. Bone Res 2023;11:11.
4. Ji T, Shi Q, Mei S, Xu J, Liang H, Xie L, et al. Integrated analysis of single-cell and bulk RNA sequencing data reveals an immunostimulatory microenvironment in tumor thrombus of osteosarcoma. Oncogenesis 2023;12:31.
5. Chen S, Zeng J, Huang L, Peng Y, Yan Z, Zhang A, et al. RNA adenosine modifications related to prognosis and immune infiltration in osteosarcoma. J Transl Med 2022;20:228.
6. Jiang Y, Wang J, Sun M, Zuo D, Wang H, Shen J, et al. Multi-omics analysis identifies osteosarcoma subtypes with distinct prognosis indicating stratified treatment. Nat Commun 2022;13:7207.
7. Zhong L, Wang J, Chen W, Lv D, Zhang R, Wang X, et al. Augmenting L3MBTL2-induced condensates suppresses tumor growth in osteosarcoma. Sci Adv 2023;9:eadi0889.
8. Han Z, Peng C, Yi J, Wang Y, Liu Q, Yang Y, et al. Matrix-assisted laser desorption ionization mass spectrometry profiling of plasma exosomes evaluates osteosarcoma metastasis. iScience 2021;24:102906.
9. Roessner A, Lohmann C, Jechorek D. Translational cell biology of highly malignant osteosarcoma. Pathol Int 2021;71:291–303.
10. Luetke A, Meyers PA, Lewis I, Juergens H. Osteosarcoma treatment—where do we stand? A state of the art review. Cancer Treat Rev 2014;40:523–32.
11. Xiao X, Wang W, Li Y, Yang D, Li X, Shen C, et al. HSP90AA1-mediated autophagy promotes drug resistance in osteosarcoma. J Exp Clin Cancer Res 2018;37:201.
12. Swift LP, Rephaeli A, Nudelman A, Phillips DR, Cutts SM. Doxorubicin–DNA adducts induce a non-topoisomerase II-mediated form of cell death. Cancer Res 2006;66:4863–71.
13. Giacomini I, Cortini M, Tinazzi M, Baldini N, Cocetta V, Ragazzi E, et al. Contribution of mitochondrial activity to doxorubicin-resistance in osteosarcoma cells. Cancers (Basel) 2023;15:1370.
14. Zhang Z, Ha SH, Moon YJ, Hussein UK, Song Y, Kim KM, et al. Inhibition of SIRT6 potentiates the anti-tumor effect of doxorubicin through suppression of the DNA damage repair pathway in osteosarcoma. J Exp Clin Cancer Res 2020;39:247.
15. Luo M, Fu A, Wu R, Wei N, Song K, Lim S, et al. High expression of G6PD increases doxorubicin resistance in triple negative breast cancer cells by maintaining GSH level. Int J Biol Sci 2022;18:1120–33.
16. Brown KK, Montaser-Kouhsari L, Beck AH, Toker A. MERIT40 is an Akt substrate that promotes resolution of DNA damage induced by chemotherapy. Cell Rep 2015;11:1358–66.
17. Wallin JJ, Guan J, Prior WW, Edgar KA, Kassees R, Sampath D, et al. Nuclear phospho-Akt increase predicts synergy of PI3K inhibition and doxorubicin in breast and ovarian cancer. Sci Transl Med 2010;2:48ra66.
18. Wegner M-S, Schömel N, Gruber L, Örtel SB, Kjellberg MA, Mattjus P, et al. UDP-glucose ceramide glucosyltransferase activates AKT, promoted proliferation, and doxorubicin resistance in breast cancer cells. Cell Mol Life Sci 2018;75:3393–410.
19. Zhai X, Xia Z, Du G, Zhang X, Xia T, Ma D, et al. LRP1B suppresses HCC progression through the NCSTN/PI3K/AKT signaling axis and affects doxorubicin resistance. Genes Dis 2023;10:2082–96.
20. Goodwin JF, Knudsen KE. Beyond DNA repair: DNA-PK function in cancer. Cancer Discov 2014;4:1126–39.
21. Mohiuddin IS, Kang MH. DNA-PK as an emerging therapeutic target in cancer. Front Oncol 2019;9:635.
22. Zenke FT, Zimmermann A, Sirrenberg C, Dahmen H, Kirkin V, Pehl U, et al. Pharmacologic inhibitor of DNA-PK, M3814, potentiates radiotherapy and regresses human tumors in mouse models. Mol Cancer Ther 2020;19:1091–101.
23. Fok JHL, Ramos-Montoya A, Vazquez-Chantada M, Wijnhoven PWG, Follia V, James N, et al. AZD7648 is a potent and selective DNA-PK inhibitor that enhances radiation, chemotherapy and olaparib activity. Nat Commun 2019;10:5065.
24. Ciszewski WM, Tavecchio M, Dastych J, Curtin NJ. DNA-PK inhibition by NU7441 sensitizes breast cancer cells to ionizing radiation and doxorubicin. Breast Cancer Res Treat 2014;143:47–55.
25. Tan KT, Yeh C-N, Chang Y-C, Cheng J-H, Fang W-L, Yeh Y-C, et al. *PRKDC*: new biomarker and drug target for checkpoint blockade immunotherapy. J Immunother Cancer 2020;8:e000485.
26. Nakamura M, Li Y, Choi B-R, Matas-Rico E, Troncoso J, Takahashi C, et al. GDE2-RECK controls ADAM10 α-secretase-mediated cleavage of amyloid precursor protein. Sci Transl Med 2021;13:eabe6178.
27. Matas-Rico E, van Veen M, Leyton-Puig D, van den Berg J, Koster J, Kedziora KM, et al. Glycerophosphodiesterase GDE2 promotes neuroblastoma

differentiation through glypican release and is a marker of clinical outcome. Cancer Cell 2016;30:548–62.
28. Feng C, Zhang L, Sun Y, Li X, Zhan L, Lou Y, et al. GDPD5, a target of miR-195-5p, is associated with metastasis and chemoresistance in colorectal cancer. Biomed Pharmacother 2018;101:945–52.
29. Cao C, Zhou S, Hu J. Long noncoding RNA MAGI2-AS3/miR-218-5p/GDPD5/SEC61A1 axis drives cellular proliferation and migration and confers cisplatin resistance in nasopharyngeal carcinoma. Int Forum Allergy Rhinol 2020;10:1012–23.
30. Zhang X, Dai X, Zhao X, Wang J, Dou J, Zhuang H, et al. MiR-874-3p represses the migration and invasion yet promotes the apoptosis and cisplatin sensitivity via being sponged by long intergenic non-coding RNA 00922 (LINC00922) and targeting glycerophosphodiester phosphodiesterase domain containing 5 (GDPD5) in gastric cancer cells. Bioengineered 2022;13:7082–104.
31. Das R, Esposito V, Abu-Abed M, Anand GS, Taylor SS, Melacini G. cAMP activation of PKA defines an ancient signaling mechanism. Proc Natl Acad Sci U S A 2007;104:93–8.
32. Patra KC, Kato Y, Mizukami Y, Widholz S, Boukhali M, Revenco I, et al. Mutant GNAS drives pancreatic tumourigenesis by inducing PKA-mediated SIK suppression and reprogramming lipid metabolism. Nat Cell Biol 2018;20:811–22.
33. Nault JC, Fabre M, Couchy G, Pilati C, Jeannot E, Tran Van Nhieu J, et al. GNAS-activating mutations define a rare subgroup of inflammatory liver tumors characterized by STAT3 activation. J Hepatol 2012;56:184–91.
34. Coles GL, Cristea S, Webber JT, Levin RS, Moss SM, He A, et al. Unbiased proteomic profiling uncovers a targetable GNAS/PKA/PP2A axis in small cell lung cancer stem cells. Cancer Cell 2020;38:129–43.e7.
35. Eisenhauer EA, Therasse P, Bogaerts J, Schwartz LH, Sargent D, Ford R, et al. New response evaluation criteria in solid tumours: revised RECIST guideline (version 1.1). Eur J Cancer 2009;45:228–47.
36. Tu C, Liu B, Li C, Feng C, Wang H, Zhang H, et al. Integrative analysis of TROAP with molecular features, carcinogenesis, and related immune and pharmacogenomic characteristics in soft tissue sarcoma. MedComm (2020) 2023;4:e369.
37. Li W, Xu H, Xiao T, Cong L, Love MI, Zhang F, et al. MAGeCK enables robust identification of essential genes from genome-scale CRISPR/Cas9 knockout screens. Genome Biol 2014;15:554.
38. Sun Y, Zhang H, Meng J, Guo F, Ren D, Wu H, et al. S-palmitoylation of PCSK9 induces sorafenib resistance in liver cancer by activating the PI3K/AKT pathway. Cell Rep 2022;40:111194.
39. Olive PL, Banáth JP. The comet assay: a method to measure DNA damage in individual cells. Nat Protoc 2006;1:23–9.
40. Nie J-H, Yang T, Li H, Li S, Li T-T, Ye H-S, et al. Frequently expressed glypican-3 as a promising novel therapeutic target for osteosarcomas. Cancer Sci 2022;113:3618–32.
41. Carter JM, Inwards CY, Jin L, Evers B, Wenger DE, Oliveira AM, et al. Activating GNAS mutations in parosteal osteosarcoma. Am J Surg Pathol 2014;38:402–9.
42. Salinas-Souza C, De Andrea C, Bihl M, Kovac M, Pillay N, Forshew T, et al. GNAS mutations are not detected in parosteal and low-grade central osteosarcomas. Mod Pathol 2015;28:1336–42.
43. Jin X, Zhu L, Cui Z, Tang J, Xie M, Ren G. Elevated expression of GNAS promotes breast cancer cell proliferation and migration via the PI3K/AKT/Snail1/E-cadherin axis. Clin Transl Oncol 2019;21:1207–19.
44. Liu Q, Turner KM, Alfred Yung WK, Chen K, Zhang W. Role of AKT signaling in DNA repair and clinical response to cancer therapy. Neuro Oncol 2014;16:1313–23.
45. Head PE, Kapoor-Vazirani P, Nagaraju GP, Zhang H, Rath SK, Luong NC, et al. DNA-PK is activated by SIRT2 deacetylation to promote DNA double-strand break repair by non-homologous end joining. Nucleic Acids Res 2023;51:7972–87.
46. Du Z, Lovly CM. Mechanisms of receptor tyrosine kinase activation in cancer. Mol Cancer 2018;17:58.
47. Wu S, Fu L. Tyrosine kinase inhibitors enhanced the efficacy of conventional chemotherapeutic agent in multidrug resistant cancer cells. Mol Cancer 2018;17:25.
48. Fang Y, Chai Z, Wang D, Kuang T, Wu W, Lou W. DNA-PKcs deficiency sensitizes the human hepatoma HepG2 cells to cisplatin and 5-fluorouracil through suppression of the PI3K/Akt/NF-κB pathway. Mol Cell Biochem 2015;399:269–78.
49. Tu Y, Ji C, Yang B, Yang Z, Gu H, Lu C-C, et al. DNA-dependent protein kinase catalytic subunit (DNA-PKcs)-SIN1 association mediates ultraviolet B (UVB)-induced Akt Ser-473 phosphorylation and skin cell survival. Mol Cancer 2013;12:172.
50. Dylgjeri E, Knudsen KE. DNA-PKcs: a targetable protumorigenic protein kinase. Cancer Res 2022;82:523–33.
51. Gill J, Gorlick R. Advancing therapy for osteosarcoma. Nat Rev Clin Oncol 2021;18:609–24.
52. Zhang J, Liu W, Zou C, Zhao Z, Lai Y, Shi Z, et al. Targeting super-enhancer-associated oncogenes in osteosarcoma with THZ2, a covalent CDK7 inhibitor. Clin Cancer Res 2020;26:2681–92.
53. Zhang W, Qi L, Liu Z, He S, Wang C-Z, Wu Y, et al. Integrated multiomic analysis and high-throughput screening reveal potential gene targets and synergetic drug combinations for osteosarcoma therapy. MedComm (2020) 2023;4:e317.